



ELSEVIER

Available online at www.sciencedirect.com

ScienceDirect

www.elsevier.com/locate/jmbbm

**Research Paper**

Targeting the finite-deformation response of wavy biological tissues with bio-inspired material architectures

**Wenqiong Tu, Marek-Jerzy Pindera***

Civil and Environmental Engineering Department, University of Virginia, Charlottesville, VA 22904-4742, United States

ARTICLE INFO**Article history:**

Received 26 May 2013

Received in revised form

29 July 2013

Accepted 1 August 2013

Available online 24 August 2013

Keywords:

Wavy microstructures

Biological tissues

Bio-inspired modeling

Micromechanics

Finite deformation

ABSTRACT

The Particle Swarm Optimization algorithm driven by a homogenized-based model is employed to target the response of three types of heart-valve chordae tendineae with different stiffening characteristics due to different degrees of waviness of collagen fibril/fiber bundles. First, geometric and material parameters are identified through an extensive parametric study that produce excellent agreement of the simulated response based on simplified unit cell architectures with the actual response of the complex biological tissue. These include amplitude and wavelength of the crimped chordae microstructure, elastic moduli of the constituent phases, and degree of microstructural refinement of the stiff phase at fixed volume fraction whose role in the stiffening response is elucidated. The study also reveals potential non-uniqueness of bio-inspired wavy microstructures in attaining the targeted response of certain chordae tendineae crimp configurations. The homogenization-based Particle Swarm Optimization algorithm, whose predictions are validated through the parametric study, is then shown to be an excellent tool in identifying optimal unit cell architectures in the design space that exhibits very steep gradients. Finally, defect criticality of optimal unit cell architectures is investigated in order to assess their feasibility in replacing actual biological tendons with stiffening characteristics.

© 2013 Elsevier Ltd. All rights reserved.

1. Introduction

Homogenization techniques play an important role in the development and design of engineered materials through establishment of direct link between function and microstructure. Specifically, they shed light on the importance of various deformation mechanisms that contribute to the macroscopic response, thereby providing an efficient virtual laboratory in support of material development, including bio-inspired architectures that mimic mechanical response of biological materials (Browning et al., 2013). The homogenization approach may also

be profitably employed in the construction of macroscopic-level, microstructure-dependent strain energy density functions for biological tissues (Garikipati et al., 2008). When the homogenization approach is combined with an optimization algorithm it has the capacity to result in a powerful and efficient identification tool for optimal bio-inspired material architectures.

We present a new homogenization-based computational technology for the identification of optimal bio-inspired material architectures that mimic the mechanical response of a class of biological tissues with wavy microstructures. These tissues serve specific functions which require tensile response

*Corresponding author. Tel.: +1 434 924 1040.

E-mail address: mp3g@virginia.edu (M.-J. Pindera).

characterized by a small initial resistance to deformation followed by a substantial increase in stiffness due to straightening of the crimped microstructure, producing limiting linear behavior. Such stiffening response is exhibited by tendons whose main load transmission mechanism is uniaxial tension supported by crimped collagen fibers oriented along the tendon's axis. The collagen fibers possess a hierarchical microstructure whose building blocks are tropocollagen molecules arranged in helical patterns that are assembled into microfibrils. Microfibrils aggregate to form bundles of fibrils that in turn form collagen fibers. Both planar and twisted arrangements of collagen fibers have been observed in different types of tendons and other biological tissues (Diamant et al., 1972; Kastelic et al., 1978; Liao et al., 2009). This, in turn, has motivated the use of the homogenization approach to simulate the response of these biological materials using planar or helical models of the crimped microstructures with varying degrees of simplifications and approximations (Comninou and Yannas, 1976; Kastelic et al., 1980; Freed and Doehring, 2005; Federico and Herzog, 2008; Gao et al., 2008; Grytz and Meschke, 2009; Khatam and Pindera, 2012). The response at the individual constituent level in these approaches has been described by continuum-based strain-energy densities such as the generalized Mooney-Rivlin model. Given the complex microstructure of collagen fibers, approaches are also pursued that incorporate atomistic considerations within hierarchical multiscale models of multiphase tissues (Buehler, 2006; Tang et al., 2009; Maceri et al., 2010).

The computational technology described herein for the identification of optimal bio-inspired wavy architectures combines the recently proposed finite-volume direct averaging micromechanics (FVDAM) theory for heterogeneous materials undergoing finite deformation (Khatam and Pindera, 2012) with the Particle Swarm Optimization (PSO) algorithm (Kennedy and Eberhart, 1995). This homogenization theory had been used in a stand-alone manner to simulate the mechanical response of a porcine mitral valve strut chordae based on a simplified model of the chordae's microstructure composed of planar alternating stiff and soft wavy layers (Khatam and Pindera, 2012). Using a trial-and-error approach, and an amplitude-to-wavelength ratio of the wavy unit cell representative of the actual crimped microstructure of the strut chordae (Liao and Vesely, 2003a), thickness and Young's modulus of the stiff and soft layers, respectively, were identified that yielded good correlation with the reported experimental response (Liao and Vesely, 2003b).

Herein, we extend this investigation by employing the FVDAM-driven PSO algorithm to identify combinations of material and geometric parameters of wavy multilayers that best fit experimental response of three types of porcine mitral valve chordae tendineae, namely marginal, basal and strut, that stiffen at increasingly greater stretches. This objective is supported by a systematic parametric study that demonstrates the importance of geometric and material parameters of model wavy multilayer architectures in simulating the stiffening response of the three chordae types. From the perspective of designing bio-inspired material architectures that accurately mimic the response of chordae tendineae for heart valve repair, planar multilayered configurations composed of alternating stiff and soft wavy layers offer the possibility of precise control of the stiffening response. Hence

they may provide an alternative to the commonly employed artificial chordae made of expanded polytetrafluoroethylene characterized by porous microstructures composed of planar random fiber arrangements. Such artificial chordae are easily infiltrated and covered by host tissue, potentially leading to long-term calcification and failure (Bortolotti et al., 2012), and the correct length determination remains an issue (Ibrahim et al., 2012). The questions relevant to the design of synthetic chordae with planar wavy architectures that this study addresses are:

- What are the effects of amplitude and period of the wavy multilayer, stiff layer thickness and phase moduli on the initial resistance to the unfolding of the wavy microstructure and subsequent stiffening response?
- Can the targeted response be attained using more than one wavy material architecture?
- How critical are the potential defects in stiff layers on the targeted response?

2. FVDAM-driven particle swarm optimization of wavy microstructure unit cells

The finite-volume direct averaging micromechanics (FVDAM) theory employs key features of the finite-volume approach implemented within the 0th-order homogenization framework (Pindera et al., 2009; Cavalcante et al., 2012). In contrast to the classical finite-volume approaches applied to both fluid and solid mechanics problems (Versteeg and Malalasekera, 2007; Demirdzic and Martinovic, 1993; Berezovski et al., 2008), FVDAM theory has been developed specifically to model materials with heterogeneous periodic microstructures (Bensoussan et al., 1978; Suquet, 1987; Charalambakis, 2010). The parametric FVDAM theory with large-deformation analysis capability was developed to model the response of biological tissues in general (Khatam and Pindera, 2012), and then applied to target the response of a porcine mitral valve strut chordae tendineae. Its accuracy in modeling the response of representative unit cells with wavy microstructures has been verified by comparison with the finite-element method (Cavalcante and Pindera, in press-a, in press-b). The semi-analytical framework of the theory facilitates implementation into higher-level analysis algorithms, such as the Particle Swarm Optimization (Kennedy and Eberhart, 1995) employed in this study. This evolutionary nongradient-based optimization algorithm successfully used in the design of flat laminates (Chen et al., 2009; Peng et al., 2011) is well-suited for problems wherein the objective function exhibits steep gradients and cusps in the design space, and hence becomes nonanalytic at those points.

The FVDAM theory generates solutions for given sets of design variables that are used in the PSO algorithm in search of the optimum set that minimizes or maximizes the specified objective function. Herein, only essential information necessary to understand how it is implemented into PSO is presented, while details of the FVDAM-based unit cell solution in the finite-deformation domain are provided in the original reference (Khatam and Pindera, 2012). Accordingly, the elastic response of a unit cell representative of a wavy multilayered material undergoing finite deformation is obtained using the total

Lagrangian formulation. It is governed by the system of equations

$$\mathbb{K} \Delta \mathbf{U}' = \mathbb{A} \Delta \bar{\mathbf{F}} \quad (1)$$

where $\Delta \mathbf{U}'$ contains common surface-averaged fluctuating displacement increments on each face of the quadrilateral subvolumes used to discretize the unit cell microstructure, \mathbb{K} is the global stiffness matrix generated by enforcing displacement and traction increment continuity conditions at adjacent subvolume faces, together with the periodicity conditions, and $\Delta \bar{\mathbf{F}}$ is the applied macroscopic deformation gradient tensor increment. \mathbb{K} contains information on the geometry of the individual subvolumes obtained from the vertex coordinates and their material constitutive parameters. Hence it needs to be reassembled if these are specified as design variables and thus altered during the search. At each applied macroscopic deformation gradient increment the solution of the global system of equations yields the unknown surface-averaged displacement increments which are employed to establish so-called localization relations for the q th subvolume (Hill, 1963):

$$\Delta \bar{\mathbf{F}}^{(q)} = \mathbb{A}^{(q)} \Delta \bar{\mathbf{F}} \quad (2)$$

where $\mathbb{A}^{(q)}$ is the elastic deformation gradient concentration tensor calculated at each loading point for the specified increment $\Delta \bar{\mathbf{F}}$. Using these relations in the definition of the volume-average first Piola-Kirchhoff stress increment $\Delta \bar{\mathbf{T}}$ expressed in terms of corresponding subdomain stress increments:

$$\Delta \bar{\mathbf{T}} = \frac{1}{V} \int_V \Delta \mathbf{T}(\mathbf{X}) dV = \frac{1}{V} \sum_{q=1}^{N_q} \int_{V_q} \Delta \mathbf{T}^{(q)}(\mathbf{X}) dV_q = \sum_{q=1}^{N_q} c_{(q)} \Delta \bar{\mathbf{T}}^{(q)} \quad (3)$$

and hence deformation gradient increments through the local constitutive equations:

$$\Delta \bar{\mathbf{T}}^{(q)} = \mathbf{R}_o^{(q)} \Delta \bar{\mathbf{F}}^{(q)} \quad (4)$$

the homogenized Hooke's law for the material-at-large is constructed in the incremental form:

$$\Delta \bar{\mathbf{T}} = \mathbf{R}^* \Delta \bar{\mathbf{F}} \quad (5)$$

where the homogenized instantaneous stiffness matrix \mathbf{R}^* is given by

$$\mathbf{R}^* = \sum_{q=1}^{N_q} c_{(q)} \mathbf{R}_o^{(q)} \mathbb{A}^{(q)} \quad (6)$$

and $c_{(q)}$ is the volume fraction of the q th subvolume. Integration of the incremental homogenized Hooke's law leads to the total stress-deformation gradient response for the specified loading that can be expressed as a stress-stretch curve typically used to report experimental data.

The PSO algorithm mimics the behavior of a swarm of birds searching for a target. The swarm consists of particles whose positions in the design variable space are employed to generate candidate solutions based on FVDAM calculations and experimental data. The position of the i th particle is given by the vector $\mathbf{X}_i = (x_1, x_2, \dots, x_D)_i$, where the subscript D represents the number of design variables, and its velocity by $\mathbf{V}_i = (v_1, v_2, \dots, v_D)_i$. During the search for an optimal solution, the particles' positions are updated based on each particle's best previous experience denoted by $p\text{Best}$ and the best experience of other particles denoted by $g\text{Best}$. The updating

algorithm is given by the two equations:

$$\begin{aligned} v_{id}^{k+1} &= \omega v_{id}^k + a_1 \text{rand}_1^k(p\text{Best}_{id}^k - x_{id}^k) + a_2 \text{rand}_2^k(g\text{Best}_{id}^k - x_{id}^k) \\ x_{id}^{k+1} &= x_{id}^k + v_{id}^{k+1} \end{aligned} \quad (7)$$

where the subscript k represents the iteration number, rand_1^k and rand_2^k are random numbers with uniform distributions in the interval [0,1], a_1 and a_2 are acceleration constants. The parameter ω is the inertia weight parameter defined in terms of its initial and final values, ω_{\max} and ω_{\min} , and the current and maximum iteration numbers k and k_{\max} ,

$$\omega = \omega_{\max} - k((\omega_{\max} - \omega_{\min})/k_{\max}) \quad (8)$$

Table 1 – Parameters used in the Particle Swarm Optimization algorithm.

a_1	a_2	ω_{\min}	ω_{\max}
2.05	2.05	0.4	0.9

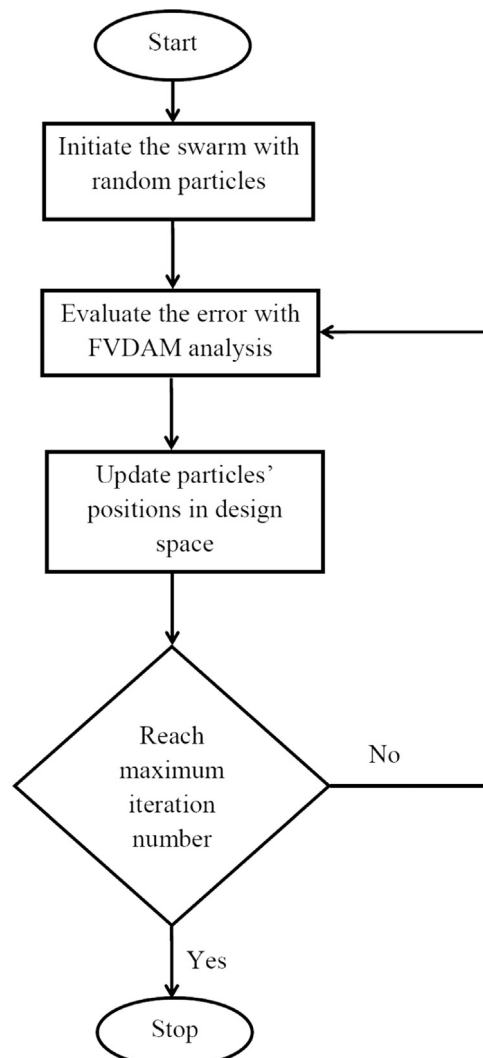


Fig. 1 – Flow chart showing the FVDAM-driven PSO.

The parameter χ introduced to ensure convergence is called constriction factor, and is defined by

$$\chi = \frac{2}{2-\varphi-\sqrt{\varphi^2-4\varphi}} \quad (9)$$

where $\varphi = a_1 + a_2$ such that $\varphi > 4$. The values of the above parameters in the present study based on the previous work (Chen et al., 2009; Peng et al., 2011) are listed in Table 1.

In the present study, the candidate solutions are error functions which are the measures of the difference between the experimental data on the longitudinal stress–stretch response $T_{22} = T_{22}(\lambda_{22})$ of three types of mitral valve chordae tendineae (Liao and Vesely, 2003b) and the predicted FVDAM response based on the simplified geometric model described in the sequel. The error functions are evaluated for each particle \mathbf{X}_i (each set of design variables) in the following manner:

$$\text{error}(\mathbf{X}_i) = \frac{\sum_{k=1}^N |(T_{22}^{\text{FVDAM}}(\mathbf{X}_i))_k - (T_{22}^{\text{exp}})_k|}{\sum_{k=1}^N (T_{22}^{\text{exp}})_k} \quad (10)$$

at $k = 1, \dots, N$ points along the $T_{22} = T_{22}(\lambda_{22})$ curve using experimental and predicted values. The error function plays the same role as the objective function employed in other optimization algorithms.

As the search for the optimum solution proceeds according to the flow chart given in Fig. 1, it is possible that some of the design variables (particle positions) may become negative. Herein, the design variables constrained to lie within specified ranges are the amplitude and wavelength of the chordae tendineae wavy multilayer unit cell models, thickness of the stiff layer and layer Young's moduli. Their values are reset to the lower and upper bounds should these values for an i th particle exceed the bounds at any iteration number during the search.

3. Model of the mitral valve chordae tendineae

Following the previous investigation (Khatam and Pindera, 2012), the complex microstructure of porcine mitral valve chordae tendineae is represented by a wavy multilayer unit cell. The construction of the simplified model for simulating the chordae response is based on the reported experimental data for this biological tissue, which includes the amplitude and wavelength ranges of the crimped collagen fibril bundles and Young's modulus ranges of the limiting tensile response of the marginal, basal and strut chordae (Liao and Vesely, 2003a). These are reproduced in Table 2. The amplitude ranges are based on SEM observations, while a polarized light

technique had been used to determine the wavelength ranges. The homogenized tensile response had been generated in an Instron machine by first preconditioning the chordae at 4 mm/s to 150 g load in a bath of Hank's solution to simulate physiological environment until the load-displacement curve became repeatable, which was followed by the actual test in the elastic range. Fig. 2 summarizes the stabilized elastic stress–strain responses of the three chordae types (reproduced from Liao and Vesely, 2003b) which will be employed for comparison with FVDAM-based simulations.

The above information is used to construct unit cells, composed of alternating wavy stiff and soft layers, Fig. 3, to target the actual response of marginal, basal and strut chordae tendineae. Such a model is obviously a simplification of the actual crimped geometry of chordae collagen fibril bundles, but the goal herein is to show that it may be successfully used to simulate the actual tensile responses of porcine mitral valve chordae tendineae upon identification of optimal geometric and material parameters. In the wavy multilayer model, the stiff phase represents the average behavior of the crimped fibril bundles, and the soft phase the ground substance, with the respective volume fractions representative of the actual biological tissue. The amplitude and wavelength of the unit cell are

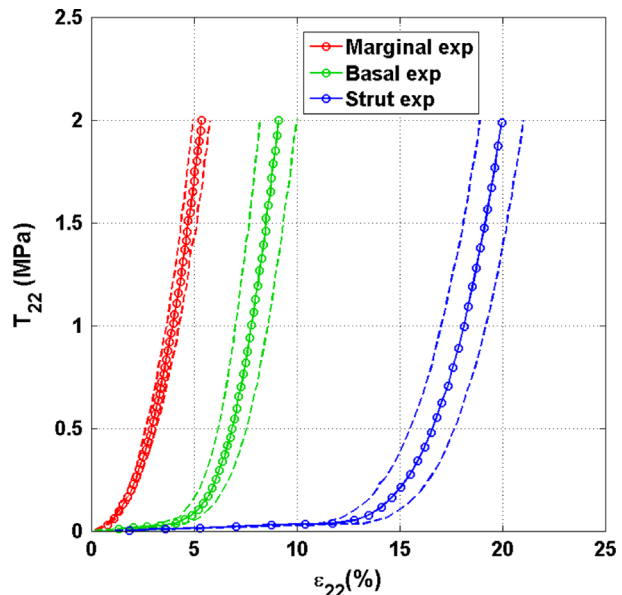


Fig. 2 – Longitudinal stress–strain response of porcine mitral valve marginal, basal and strut chordae tendineae (reproduced by digitization from the experiment data of Liao and Vesely, 2003b).

Table 2 – Ranges of the amplitude and wavelength of the crimped microstructure of the porcine mitral valve marginal, basal and strut chordae tendineae and Young's modulus of the limiting linear response (Liao and Vesely, 2003a) employed in the construction of unit cell models and the extraction of hyperelastic constitutive model parameters.

Chordae type	Amplitude (μm)	Wavelength (μm)	E_{chordae} (MPa)
Marginal	1.87 ± 0.78	14.8 ± 3.0	84.4 ± 21.2
Basal	1.87 ± 0.78	14.8 ± 3.0	86.1 ± 20.9
Strut	1.87 ± 0.78	11.3 ± 1.4	64.2 ± 13.5

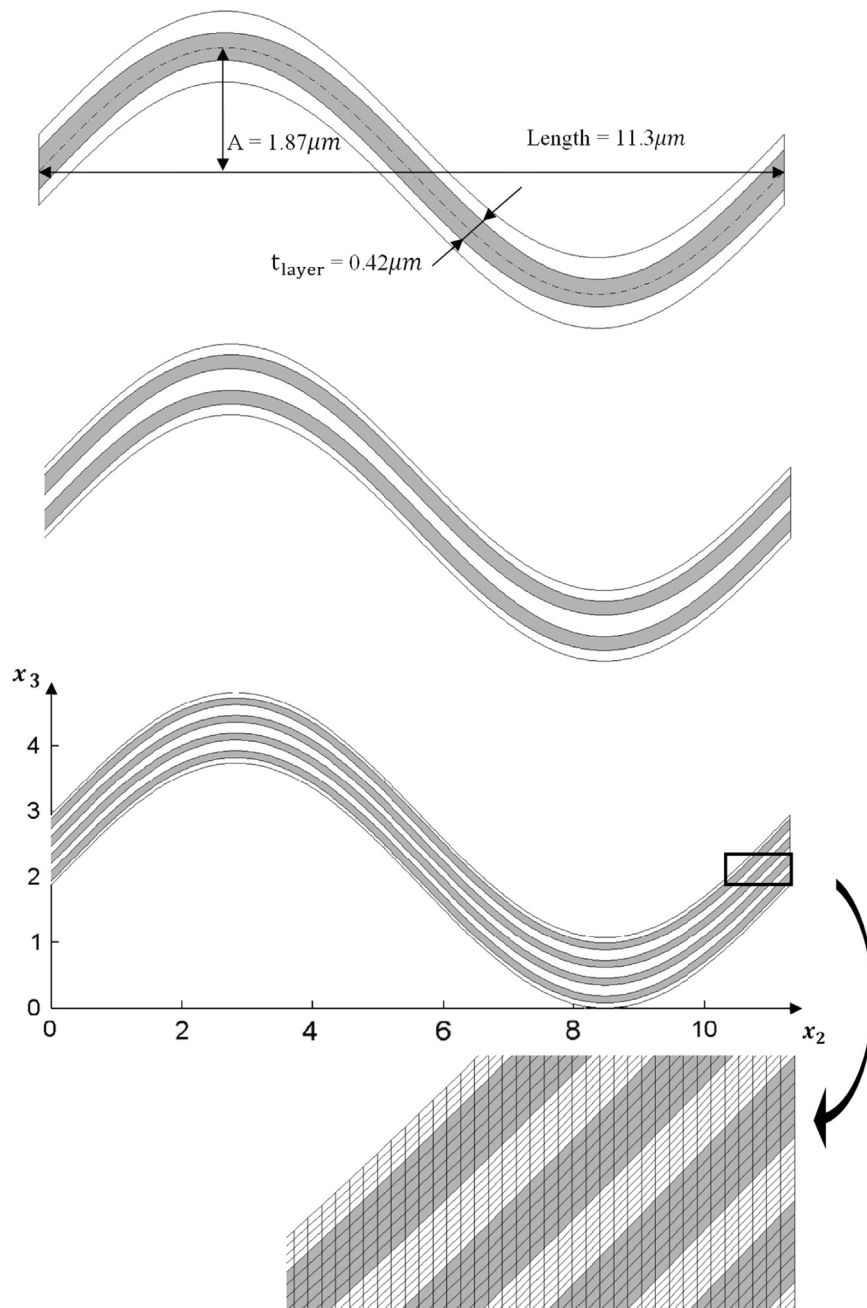


Fig. 3 – Geometry of the simplified model of the microstructure of porcine mitral valve strut chordae employed in the FVDAM simulations based on the reported mean values of amplitude and crimp period (Liao and Vesely, 2003a). The top representative unit cell is the reference cell with thickest stiff layer which is further subdivided in a manner that retains its volume fraction (middle and bottom unit cells). Detail of the unit cell discretization is shown in the bottom unit cell (note: axes scale is in microns).

varied according to the experimental data in Table 2. The thickness of the reference stiff layer, $0.42 \mu\text{m}$, is the same as in the previous study (Khatam and Pindera, 2012). Given that the fibril diameter within fibril sub-bundles of the crimped marginal, basal and strut chordae lies in the range 45–60 nm (Liao and Vesely, 2003a), the thickest stiff layer corresponds to about 7–9 fibril diameters. The overall thickness of the unit cell is adjusted such that the overall stiff layer volume fraction is fixed at 0.48 as reported (Liao and Vesely, 2003a), with the length dependent on

the crimp period. The microstructural refinement of the reference unit cell is attained by subdividing the thick stiff layer into progressively thinner ones, with the maximum number of subdivisions producing 8 stiff layers and the thinnest stiff layer thickness on the order of a single fibril diameter.

While the previous study (Khatam and Pindera, 2012) was limited to the effect of soft layer modulus and stiff layer thickness in the simulation of porcine mitral valve strut chordae using mean values of the reported amplitude-to-wavelength

ratio of the crimped fibril microstructure and Young's modulus of the limiting chordae response, the present study is much broader. It includes the effects of variations of amplitude, period, soft and stiff layer Young's moduli as well as microstructural refinement for all three chordae models.

3.1. Unit cell discretization

The reference unit cell with a single stiff layer for the marginal and basal chordae is generated using mesh discretization of 468×24 quadrilateral subvolumes along the horizontal and vertical directions, respectively. This discretization ensures that the aspect ratio of each subvolume is not excessively large. Similarly, the reference unit cell for the strut chordae is discretized into 312×24 subvolumes due to smaller crimp period. Microstructural refinement is accomplished in a manner that ensures that the overall unit thickness, stiff layer volume fraction and amplitude-to-wavelength ratio remain fixed. In this case, the smallest unit cell for the given refinement is employed. For instance, the smallest unit cell for the marginal and basal chordae with the thick stiff layer subdivided into 8 thinner ones contains a single thin stiff layer which requires the discretization of 1080×14 to maintain a reasonable subvolume aspect ratio. A full unit cell containing 8 thin stiff layers would be discretized into 1080×112 subvolumes. The corresponding discretization for the smallest strut chordae unit cell containing one thin stiff layer is 720×14 in contrast with 720×112 subvolumes for the full unit cell with 8 thin stiff layers.

3.2. Phase constitutive response

Both the stiff and soft phases of the wavy multilayer model, that represent collagen fibril bundles and ground substance material with complicated microstructure composed of randomly oriented network of collagen filaments (elastin) embedded in a hydrated proteoglycan gel producing soft and isotropic matrix, are represented by the generalized Mooney–Rivlin material. The strain energy density function for this material model is given in terms of the three invariants of the right-Cauchy deformation tensor \mathbf{C} , $I_1 = \text{tr } \mathbf{C}$, $I_2 = \frac{1}{2}(\text{tr}^2 \mathbf{C} - \text{tr } \mathbf{C}^2)$, $I_3 = \det \mathbf{C}$,

$$W = c_1 \left(\frac{I_1}{I_3^{1/3}} - 3 \right) + c_2 \left(\frac{I_2}{I_3^{2/3}} - 3 \right) + \frac{\kappa}{2}(J-1)^2 \quad (11)$$

where $J = \det \mathbf{F} = \sqrt{I_3}$, c_1 and c_2 are material parameters with $c_1 + c_2 = \mu/2$, and μ and κ are shear and bulk moduli, respectively. The compressibility or Poisson's ratio may be changed by assigning different values for $\kappa = 2\mu(1+\nu)/3(1-2\nu)$. This hyperelastic

constitutive model is often used for soft materials because of the control of the amount of compressibility.

Young's modulus ranges of the stiff layers, which represent the crimped bundles of collagen fibrils in the considered mitral valve marginal, basal and strut chordae tendineae, are determined from the limiting linear response of the experimentally determined chordae stress-strain curves, Table 2. The individual fibrils within the fiber bundles are assumed to have straightened when the chordae stiffening response becomes linear. Using the chordae Young's modulus ranges listed in Table 2, the volume fraction of collagen fibrils of 0.48, and the rule-of-mixtures formula based on the assumption of negligible contribution from the ground substance, Young's modulus ranges of the stiff layers in the simplified wavy model are thus obtained and listed in Table 3. The knowledge of Young's moduli, together with an assumed Poisson's ratio of 0.30 allows one to calculate the initial shear modulus ranges from the isotropic relation $\mu = E/2(1+\nu)$ and hence the bulk modulus ranges. Taking $c_2 = 0$ as in the previous study (Khatam and Pindera, 2012), which in fact reduces the generalized Mooney–Rivlin material to a compressible neo-Hookean one, all the required material parameters needed in Eq. (11) are obtained. The stiff layer parameter ranges thus extracted from the marginal, basal and strut chordae response are included in Table 3.

The following assumption and approximation intrinsic to the above calculations need to be highlighted. The stiff layers in the wavy multilayer model are taken as isotropic, while the microstructure of collagen fibrils suggests, at least, transversely isotropic properties. However, the soft layers representing the ground substance are not expected to significantly affect the transverse deformation of the stiff layers under longitudinal loading because the major stress component controlling the unfolding and stiffening of the wavy microstructure is along the applied load. Hence the transverse properties of the stiff layers will have a minimal influence on the axial deformation of the chordae which is the focus in the present study. Clearly, this model will not be accurate under multiaxial loading of the considered chordae tendineae which would require accurate transverse fibril properties to be realistic. Hence the extraction of the constituent phase properties in the manner described above limits the model to longitudinal loading, the primary loading for the considered tissue. This circumvents the issue of incompressibility assumed for many biological tissues under multiaxial loading, and supports the choice for Poisson's ratio values of the stiff and soft layers representative of many polymers.

Table 3 – Elastic parameters of the generalized Mooney–Rivlin model extracted from the experimental data on the porcine mitral valve marginal, basal and strut chordae tendineae (Liao and Vesely, 2003a) employed in the simplified unit cell models for the response of chordae tendineae constituents. The marginal, basal and strut layers are the stiff layers in the simplified model and the matrix is the soft layer.

Material	E (MPa)	ν	κ (MPa)	c_1 (MPa)	c_2 (MPa)
Marginal layer	175.83 ± 44.16	0.30	146.53 ± 36.81	33.81 ± 8.49	0.0
Basal layer	179.37 ± 43.54	0.30	149.48 ± 36.28	34.49 ± 8.37	0.0
Strut layer	133.75 ± 28.12	0.30	111.46 ± 23.44	25.72 ± 5.41	0.0
Matrix	0.1	0.30	0.083	0.019	0.0

4. Numerical results

Given the reported variations in the crimp geometry and elastic moduli of the porcine mitral valve chordae, [Table 2](#), the focus is first placed on parametric studies that lead to the identification of geometric and constitutive parameters in the simplified unit cell models which provide the best fit to the experimental data, [Fig. 2](#). To accomplish this, we employ the error function given by Eq. (10) which also serves as the objective function in the PSO algorithm and evaluate it for different material and geometric parameters within the reported ranges specified in [Tables 2](#) and [3](#). We first investigate the effect of amplitude and crimp period or wavelength variation on the homogenized response of the three chordae unit cell models to identify those combinations that minimize the above error, and then address the effects of constituent moduli and microstructural refinement. Optimization studies that minimize the above error function based on the PSO algorithm are then conducted in the three-dimensional design variable space with the coordinates representing the two constituent phase moduli and the number of stiff phase layers at fixed volume fraction through successive layer subdivision. The best magnitudes of amplitudes and periods identified in the parametric study are employed in the PSO optimization studies. Finally, defect criticality of the optimum unit cell architectures is investigated by maximizing the homogenized response deviation from the experimental data for different number of stiff layer fractures using the above error function. The design variables in this case are the fracture locations.

4.1. Crimp amplitude and wavelength sensitivity study

The amplitude and wavelength sensitivity study for the model chordae unit cells is performed based on the mean values of the tensile modulus for each chordae type which produce the stiff layer moduli given in [Table 3](#), the same matrix (or soft layer) modulus of 0.1 MPa, and a unit cell containing 4 stiff layers obtained from the reference unit cell using the described microstructural refinement. These baseline parameters are motivated by the previous study that was limited to the strut chordae tendineae ([Khatam and Pindera, 2012](#)).

[Fig. 4](#) illustrates the error variation as a function of the crimp amplitude and wavelength for the three chordae tendineae. For the marginal chordae model, the smallest error of 0.48 or deviation from the experimental data occurs for the amplitude of 1.09 μm and wavelength of 17.8 μm which yield amplitude-to-wavelength ratio of 0.0612. For the basal chordae model, small errors appear along an inclined trough or line in the amplitude-wavelength plane that produces amplitude-to-wavelength ratios in the range 0.082–0.083. In particular, the smallest error of 0.0425 occurs for the amplitude of 1.48 μm and wavelength of 17.8 μm. Slightly greater errors of 0.0661 and 0.1224 are obtained for the amplitudes of 1.285 and 1.09 μm, and the corresponding wavelengths of 15.5 and 13.3 μm, respectively. We observe similar error function shape in the case of strut chordae model where smallest errors are obtained for the amplitude-to-wavelength ratios around 0.135 along an inclined line in the amplitude-wavelength plane. There are two locations with the smallest error of 0.1 produced by the amplitudes of 1.48 and 1.675 μm and

the corresponding wavelengths of 10.95 and 12.35 μm, yielding respective ratios of 0.1352 and 0.1356.

[Fig. 5](#) illustrates the homogenized stress–stretch responses of the three chordae models based on the amplitudes and wavelengths that produce the smallest errors. Also included in the respective figures are responses for those combinations of amplitudes and wavelengths, denoted by solid black lines, that produce the greatest deviation from the experimental data in the considered parameter ranges. Comparison with the smallest-error curves quantifies the error magnitudes vis-a-vis the homogenized response ranges for the three chordae types. In the case of the marginal chordae model, the predicted homogenized response exhibits limiting response which is nearly parallel to the experimental data, but the initial response is too compliant leading, in turn, to stiffening at higher stretches. Prior work ([Khatam and Pindera, 2012](#)) suggests that the excessively compliant response during the unfolding process of the wavy microstructure may be corrected by increasing the matrix modulus. In contrast, the basal chordae model response based on the identified amplitude and wavelength is already very close to the experimental data, suggesting a smaller adjustment in the matrix modulus and/or microstructural refinement in order to slightly increase the extensibility. The strut chordae model response based on the identified amplitude and wavelength is also close to the experimental data, but further reduction in error requires adjusting both the matrix and stiff layer moduli, as well as microstructural refinement.

The simulated responses with greatest deviation from the experimental data indicate that substantial scatter in the predicted stress–stretch curves may be expected within the reported parameter variation ranges. For the marginal chordae model, the worst combination of amplitude and crimp period produces a response that does not capture the stiffening response of the actual tissue at all. Stiffening is observed in the case of the basal and strut chordae models, but it is premature, leading to large deviations from the experimental data. In particular, the response based on the parameters that produce the greatest error for the strut chordae model underestimates the extensibility to such a large extent that it is closer to the experimental response of the basal chordae.

4.2. Layer thickness and matrix modulus sensitivity study

Using the amplitude and wavelength values of wavy unit cells that produce the smallest homogenized response deviation from the experimental data, we investigate the effects of phase moduli and microstructural refinement on further error reduction. At first, we keep the stiff layer modulus E_f fixed at mean values for the three types of chordae and vary the matrix modulus E_m and the number of progressively thinner stiff layers at the fixed volume fraction of 0.48 and unit cell thickness H . The matrix modulus range based on the previous study of [Khatam and Pindera \(2012\)](#) is [0.05, 1.25] MPa, and the number of stiff layers lies in the range [1, 8].

The corresponding error graphs in the $E_f/E_m - H/t_{layer}$ plane for the three chordae unit cell models are shown in [Fig. 6](#). For the marginal chordae model, the smallest errors are observed for large values of the matrix modulus in the specified range where little effect of the layer thickness is observed. In contrast, the smallest errors for the basal and strut chordae

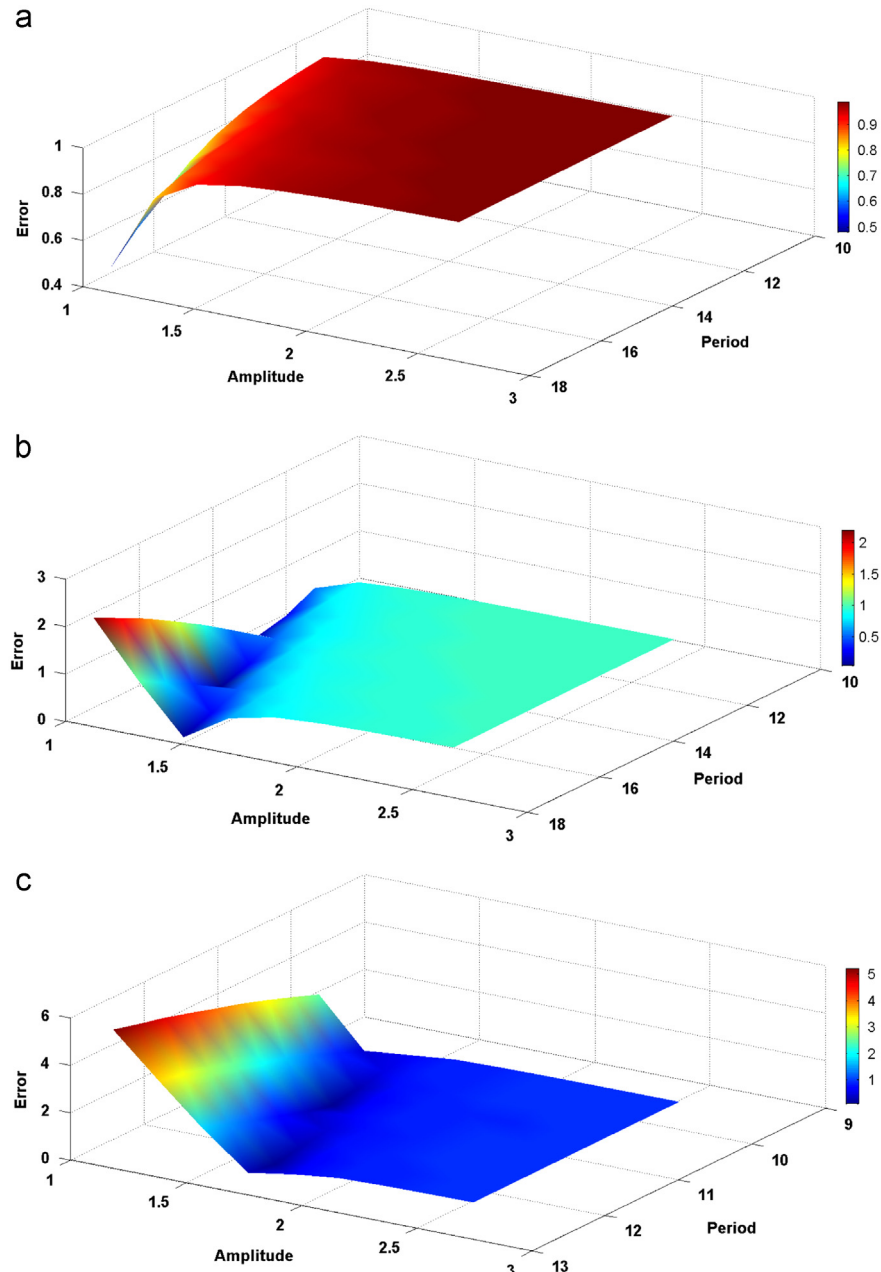


Fig. 4 – The effect of crimp amplitude and period of the wavy chordae tendineae microstructure on the homogenized response error relative to the experimental data (Liao and Vesely, 2003b) for the three types of chordae tendineae: (a) marginal; (b) basal; and (c) strut. Mean values of the stiff layer modulus for each chordae type and unit cells composed of four stiff layers were used in the simulations. (a) $E_f=175.83$ MPa, $E_m=0.1$ MPa. (b) $E_f=179.37$ MPa, $E_m=0.1$ MPa. (c) $E_f=133.75$ MPa, $E_m=0.1$ MPa.

models occur when the matrix modulus is very small, and the number of layers becomes sufficiently large. Further error reductions may be realized by first examining the homogenized stress–stretch responses based on the values of the matrix moduli and stiff layer numbers identified from the above graphs.

Fig. 7 presents the homogenized stress–stretch responses for the marginal chordae model, illustrating the parameter variation procedure that ultimately produces the best correlation with the experimental data. The homogenized responses for the unit cells with 1 and 4 stiff layers and the corresponding

matrix moduli of $E_m = 1.1$ and 1.25 MPa are compared with the experimental data in Fig. 7a. Varying the two parameters in the above manner produces an essentially the same response which is slightly too stiff during the initial unfolding process and slightly too compliant in the limit when the crimped microstructure has straightened out. Increasing the number of layers to 8 while keeping the matrix modulus fixed at $E_m = 1.25$ MPa in order to further increase the compliance during the unfolding process does not substantially improve the initial response, Fig. 7b. On the other hand, increasing the stiff layer modulus from its mean value to the maximum in the

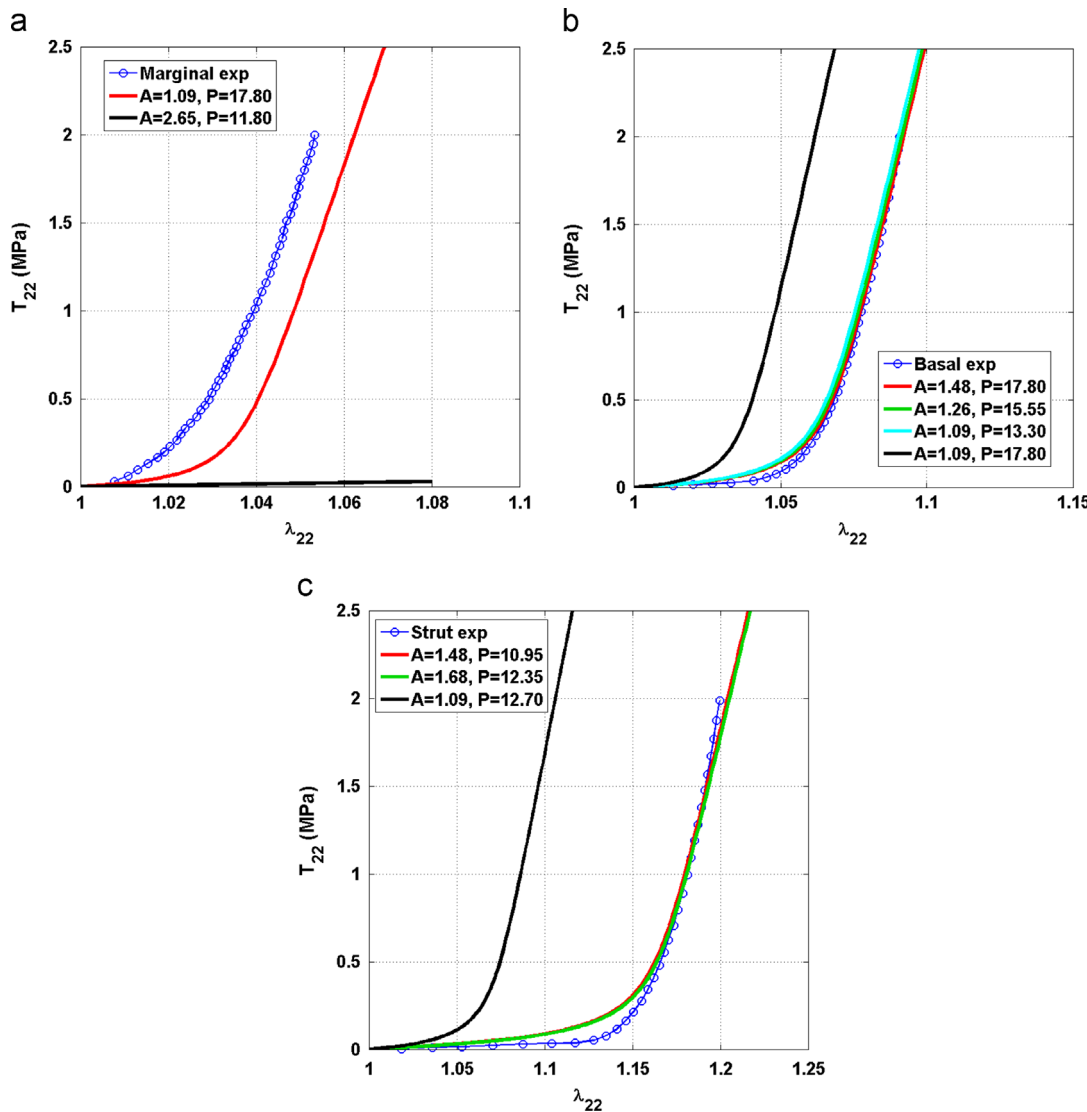


Fig. 5 – Simulated homogenized response of marginal (a), basal (b) and strut (c) chordae tendineae with amplitude and wavelength geometry that minimizes the error relative to the experimental data (Liao and Vesely, 2003b) based on reference material moduli of soft and stiff layers and unit cell composed of four stiff layers. The black solid curves included for reference represent responses that maximize the error.

considered range brings the limiting response in almost perfect coincidence with the experimental data, as observed in Fig. 7e which illustrates the effect of stiff layer modulus variation for the unit cell with 4 stiff layers and matrix modulus of $E_m = 1.25$ MPa. The final adjustment required to improve the initial response is carried out by progressively lowering the matrix modulus with the stiff layer modulus fixed at the upper bound and the unit cell discretized into 4 stiff layers, Fig. 7d. As observed in the figure, excellent agreement with the experimental data is obtained when the matrix modulus is reduced to $E_m = 0.75$ MPa.

Figs. 8 and 9 present the homogenized responses of basal and strut chordae unit cell models using the best parameters obtained from the layer thickness and matrix modulus sensitivity study, and subsequent variation in the stiff layer modulus. For the basal chordae model, excellent agreement with the experimental data is obtained for the lowest matrix

modulus of $E_m = 0.05$ MPa and the mean stiff layer modulus $E_f = 179.37$ MPa using unit cells discretized into 3 or 8 layers, with respective errors of 0.0256 and 0.0325. The corresponding responses are visually indistinguishable, Fig. 8a. Hence no additional adjustment of the stiff layer modulus is necessary as observed in Fig. 8b which illustrates the effect of varying the stiff layer modulus in the aforementioned range on the homogenized response. The results for the strut chordae model are presented in Fig. 9 where further improvement in the targeted response may be attained by identifying the stiff layer modulus E_f between the mean and upper bound values.

4.3. Targeting the response using particle swarm optimization

The results of the parametric sensitivity studies provide insight into the effects of the considered geometric and

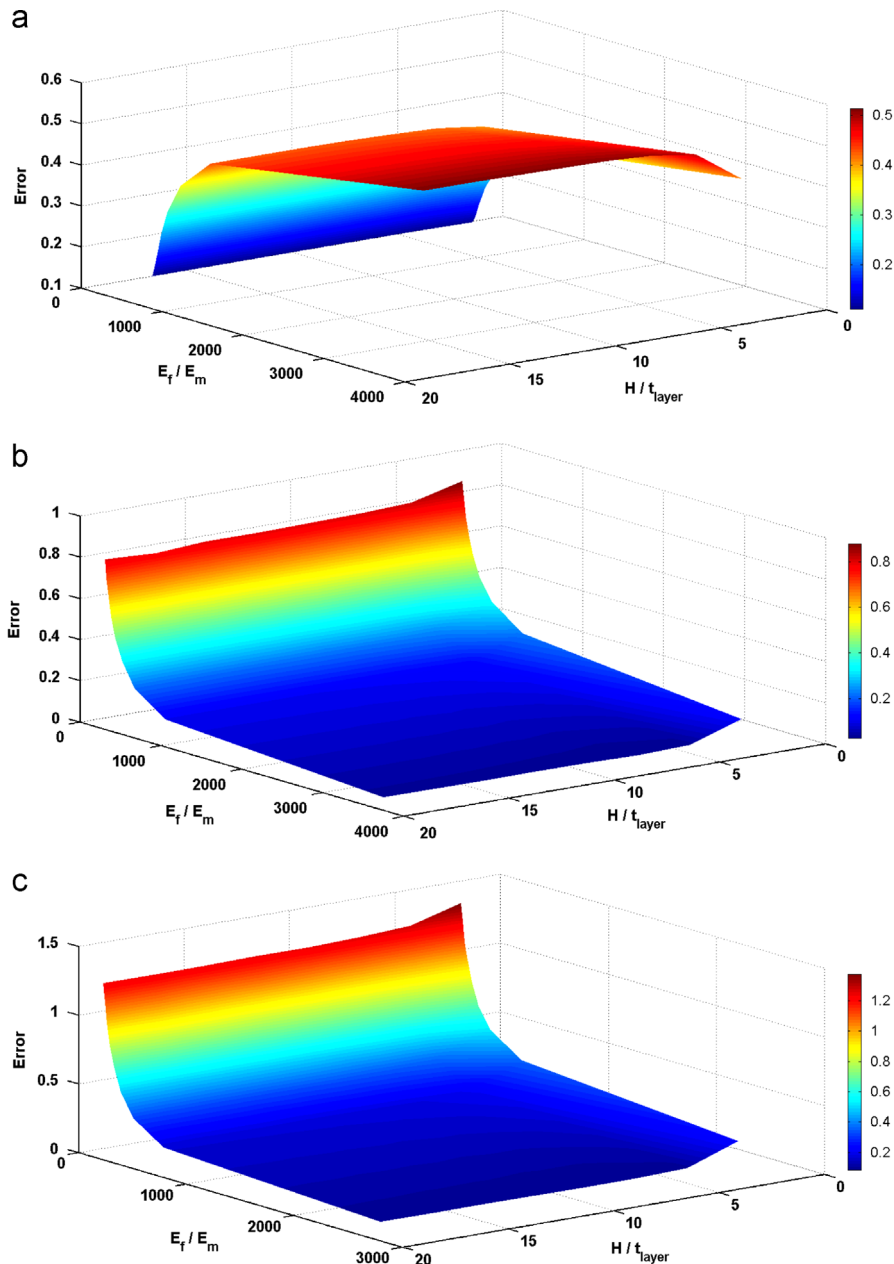


Fig. 6 – The effect of matrix Young's modulus relative to fixed stiff layer modulus and layer thickness of the wavy chordae tendineae microstructure on the homogenized response error relative to the experimental data (Liao and Vesely, 2003b) for the three types of chordae tendineae: (a) marginal; (b) basal; and (c) strut. Unit cells with optimal amplitude-to-wavelength ratios were used in the simulations. (a) $E_f = 175.83$ MPa. (b) $E_f = 179.37$ MPa. (c) $E_f = 133.75$ MPa.

material parameters of the unit cell models on the deformation mechanism of bio-inspired materials with wavy microstructures involving the unfolding and subsequently stiffening of the crimped constituents. They also serve as a reference against which optimization results may be compared and validated. Initial validation was accomplished in the amplitude-wavelength design variable space with the same parameters as the ones used to generate Fig. 4. For the marginal chordae model, unique combination of the design variables consistent with the sensitivity study was correctly identified. Similarly, for the basal and strut chordae models

where multiple sets of design variables minimize the error function, multiple sets were identified consistent with the sensitivity studies which produced the same amplitude-to-wavelength ratios.

Next, we present detailed results of optimization studies using fixed amplitude and wavelength values identified in the initial sensitivity and optimization studies that minimize the error in the predicted homogenized response for the three chordae types. The amplitudes are 1.09, 1.48 and 1.675 μm for the marginal, basal and strut chordae models, respectively, with the corresponding wavelengths set at 17.8, 17.8, and

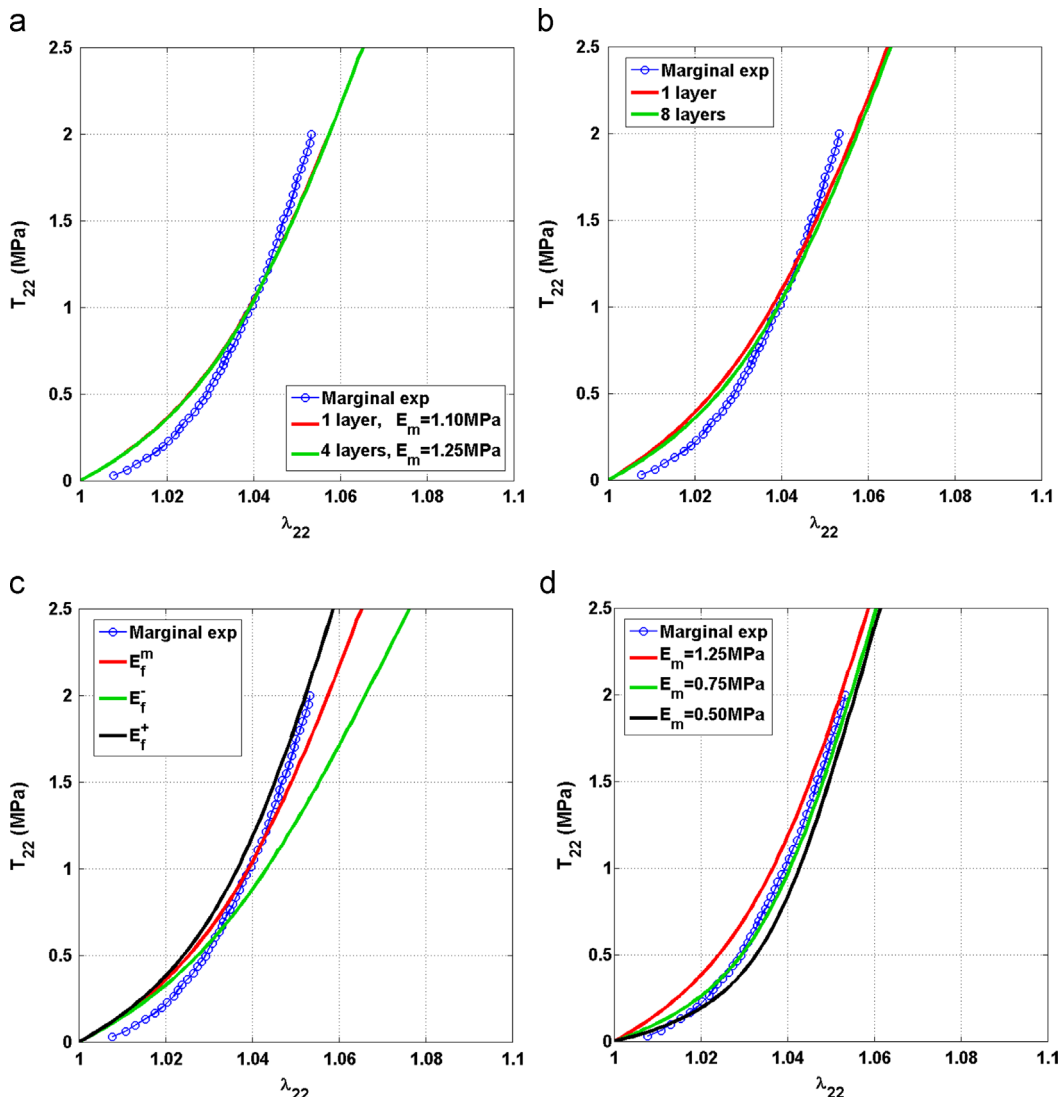


Fig. 7 – The effects of soft and stiff layer Young's moduli E_m, E_f , respectively, and stiff thickness on the simulated homogenized response of marginal chordae tendineae for the unit cell with the amplitude of $1.09 \mu\text{m}$ and wavelength of $17.8 \mu\text{m}$: (a) $E_f^{mean} = 175.83 \text{ MPa}$; (b) $E_f^{mean} = 175.83 \text{ MPa}$; (c) $E_f = 175.83 \pm 44.16 \text{ MPa}$, $E_m = 1.25 \text{ MPa}$ and unit cell composed of four stiff layers; (d) $E_f^+ = 182.99 \text{ MPa}$ and unit cell composed of four stiff layers. The superscripts “+” and “−” represent extreme values of the stiff (fiber) layer Young's moduli in the given range, Table 3.

12.35 μm . Thus the design variables for the three chordae models are the number of stiff layers in the range [1,8] at fixed volume fraction, the matrix modulus E_m which lies in the range [0.05,1.25] MPa, and the stiff layer modulus E_f with ranges dependent on the chordae. For the marginal chordae the range of E_f is [130,220] MPa, while for the basal and strut chordae the respective ranges are [136,223] MPa and [106,162] MPa. The objective function in all cases is the previously defined error that minimizes deviation of the predicted response from the experimental data (Liao and Vesely, 2003b). The number of particles used in the optimization runs was 12 and the number of allowed iterations was 14, which was sufficient to obtain converged results. Fig. 10 illustrates the error convergence as a function of iteration number for the three chordae models. Detailed results follow.

Fig. 11 illustrates the results of the optimization process for the marginal chordae model, which include the initial and final particle distributions in the three-dimensional design variable space, and the initial and converged homogenized responses after 10 iterations. The error decreases from an initial value of 0.080 to the final value of 0.036 with the concomitant design variable changes from $E_m = 0.959$, $E_f = 197.0$ and 6 stiff layers to the final values of $E_m = 0.912$, $E_f = 219.2$ and 8 stiff layers. We note that each set of results represents the design variables that produce the best solution of the entire twelve-particle swarm for the given iteration. The above results compare well with the results of the sensitivity studies followed by a more intuitive procedure that produced the best homogenized response for the set of design variables given by $E_m = 0.75$ and $E_f = 219.58 \text{ MPa}$ and 4 stiff layers.

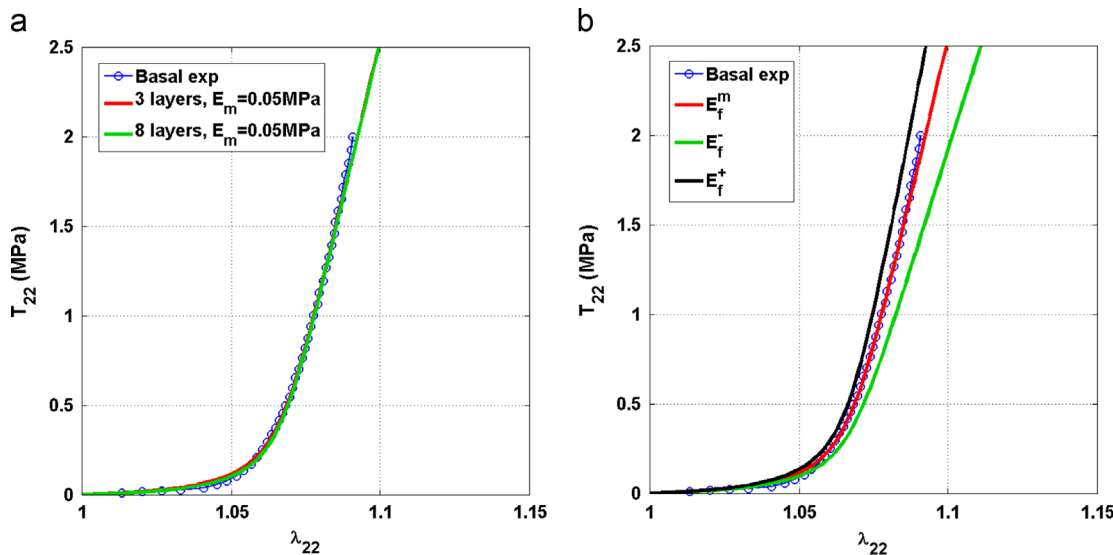


Fig. 8 – The effect of soft and stiff layer Young's moduli E_m, E_f , respectively, and stiff layer thickness on the simulated homogenized response of basal chordae tendineae for the unit cell with the amplitude of $1.48 \mu\text{m}$ and wavelength of $17.8 \mu\text{m}$: (a) $E_f^{\text{mean}} = 179.37 \text{ MPa}$; (b) $E_f = 179.37 \pm 43.54 \text{ MPa}$, $E_m = 0.05 \text{ MPa}$ and unit cell composed of three stiff layers. The superscripts “+” and “-” represent extreme values of the stiff (fiber) layer Young's moduli in the given range, Table 3.

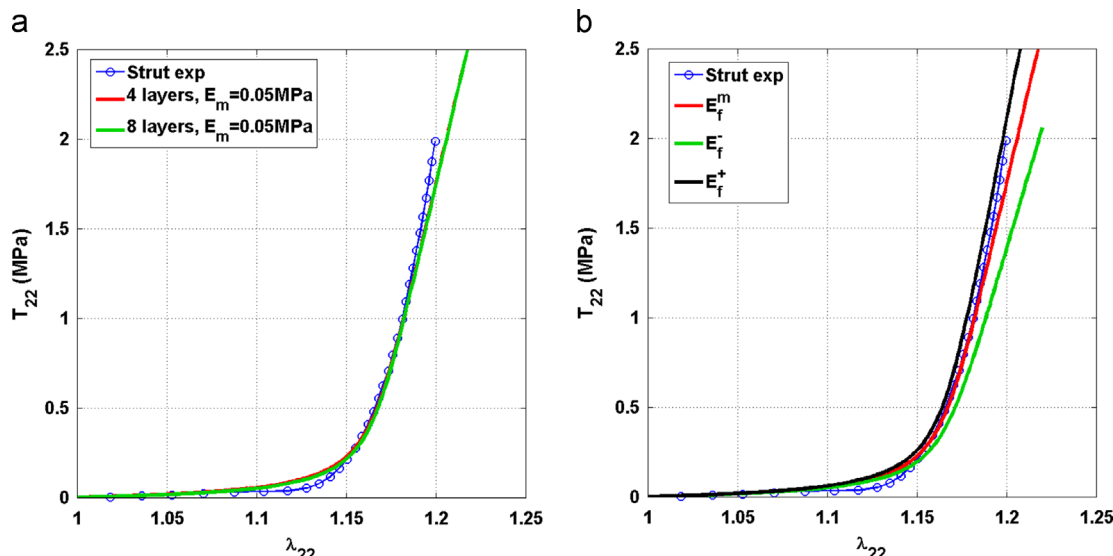


Fig. 9 – The effect of soft and stiff layer Young's moduli E_m, E_f , respectively, and stiff layer thickness on the simulated homogenized response of strut chordae tendineae for the unit cell with the amplitude of $1.67 \mu\text{m}$ and wavelength of $12.7 \mu\text{m}$: (a) $E_f^{\text{mean}} = 133.75 \text{ MPa}$; (b) $E_f = 133.75 \pm 28.12 \text{ MPa}$, $E_m = 0.05 \text{ MPa}$ and unit cell composed of four stiff layers. The superscripts “+” and “-” represent extreme values of the stiff (fiber) layer Young's moduli in the given range, Table 3.

Figs. 12 and 13 present the corresponding results for the basal and strut chordae models, respectively. For the basal chordae model, only 5 iterations are required to obtain converged homogenized response that minimizes the error relative to the experimental data, with the initial error of 0.11 after the first iteration decreasing to 0.0223. The swarm of particles with an initially random distribution in the three-dimensional design variable space converges to a very small cluster upon final iteration, Fig. 12a. The best of the initial set of design variables after the first iteration, composed of $E_m = 0.088$, $E_f = 159.95 \text{ MPa}$ and 6 stiff layers, produces a

slightly stiffer initial and a more compliant limiting response relative to the experimental data. Reduction and increase in the matrix and stiff layer moduli, respectively, yield an optimal set of design variables with the best solution composed of $E_m = 0.05$, $E_f = 185.14 \text{ MPa}$ and 7 stiff layers which yield an excellent agreement with the experimental data, Fig. 12b. These values compare well with those obtained from the parametric sensitivity studies based on the optimal amplitude and wavelength identified for the basal chordae model which yielded $E_m = 0.05$, $E_f = 179.37 \text{ MPa}$ with the number of stiff layers varying between 3 and 8.

The initial and final design variable distributions and the corresponding homogenized responses for the strut chordae model are shown in Fig. 13. The best of the initial set of design variables whose distribution is shown in Fig. 13a produces an error of 0.145 based on the values of $E_m = 0.115$, $E_f = 135.48$ MPa and 2 stiff layers. This initial set does not capture well enough the initially compliant response, Fig. 13b, owing to the large bending stiffness and hence resistance of the relatively thick stiff layers during the unfolding process. The final particle swarm converges to a small cluster in the design variable space with the best set of values given by $E_m = 0.05$, $E_f = 147.51$ MPa and 8 stiff layers. These values produce an error of 0.0377 between the predicted homogenized response and the experimental data which exhibit excellent correlation. They also compare well with

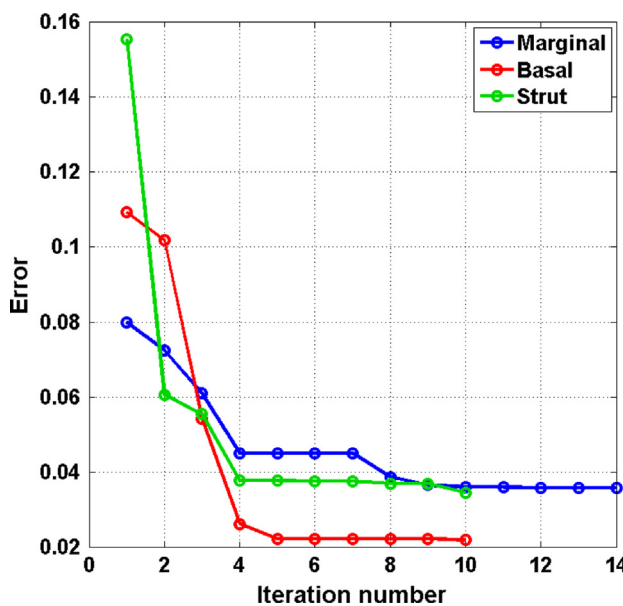


Fig. 10 – The error convergence with iteration number of the PSO algorithm in simulating the homogenized response of porcine mitral valve marginal, basal and strut chordae.

those obtained from the parametric sensitivity studies which yielded $E_m = 0.05$, $E_f = 133.75$ – 161.00 MPa with the number of stiff layers varying between 4 and 8.

4.4. Defect criticality of optimal unit cell architectures

During the unfolding process of the wavy microstructure stress gradients due to local bending develop in the crest and trough regions that may lead to localized fractures. The magnitude of the maximum stresses in these regions depends on the layer's moment of inertia and stiffness. Even in the case of thin layers such as those in a 17-layer unit cell composed of alternating soft and stiff phases, the stress gradient reversal during cyclic loading may lead to fatigue-induced crack initiation and localized fracture. Moreover, intrinsic defects may be present at other locations owing to manufacturing process and/or material variability. Hence it is important to address the question of the effect of localized stiff layer fractures on the deviation from the homogenized response relative to the response of unit cells with intact layers and optimal properties. We address this issue by maximizing the error function defined previously for different numbers of stiff layer fractures, with fracture locations playing the role of design variables, for the identified unit cell architectures that mimic the homogenized response of marginal, basal and strut chordae tendineae.

Fig. 14 illustrates the simulated homogenized response of the marginal chordae tendineae as a function of stiff layer breaks that maximize the error function. Included in the figure are the normal and shear stress distributions in the unit cell with 7 breaks which identify fracture locations, and comparison with the corresponding distributions in the unit cell configuration to stiff layer fractures is quite high up to about 7 fractures. The normal stress transfer at the fiber breaks to adjacent fibers as well as into the affected fibers away from the breaks is quite effective through the well-known shear-lag mechanism owing to the relatively high matrix modulus, as observed in the normal and shear stress distributions.

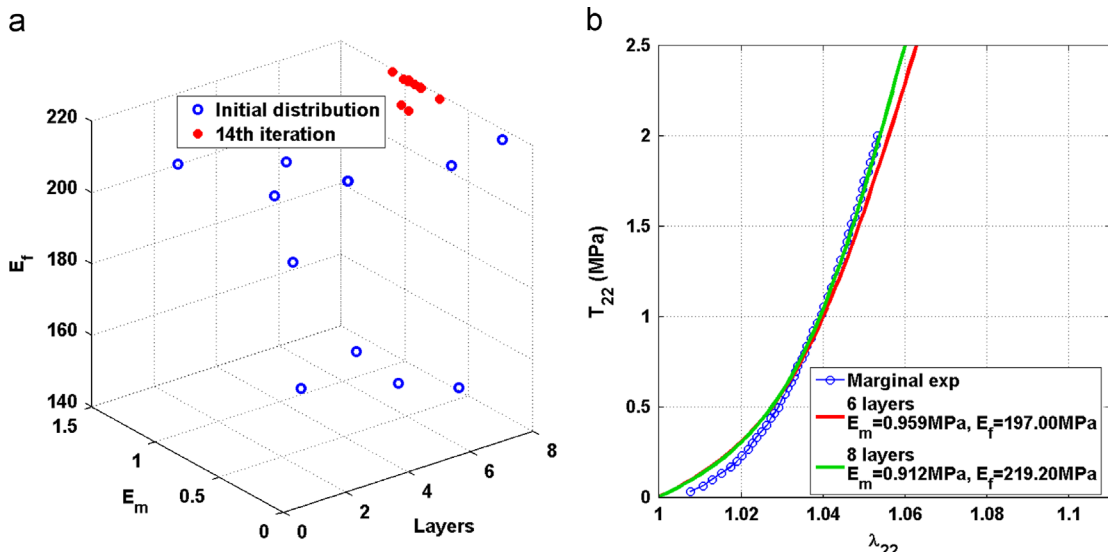


Fig. 11 – (a) Initial and final particle distributions. (b) Best initial and final homogenized responses of the marginal chordae tendineae.

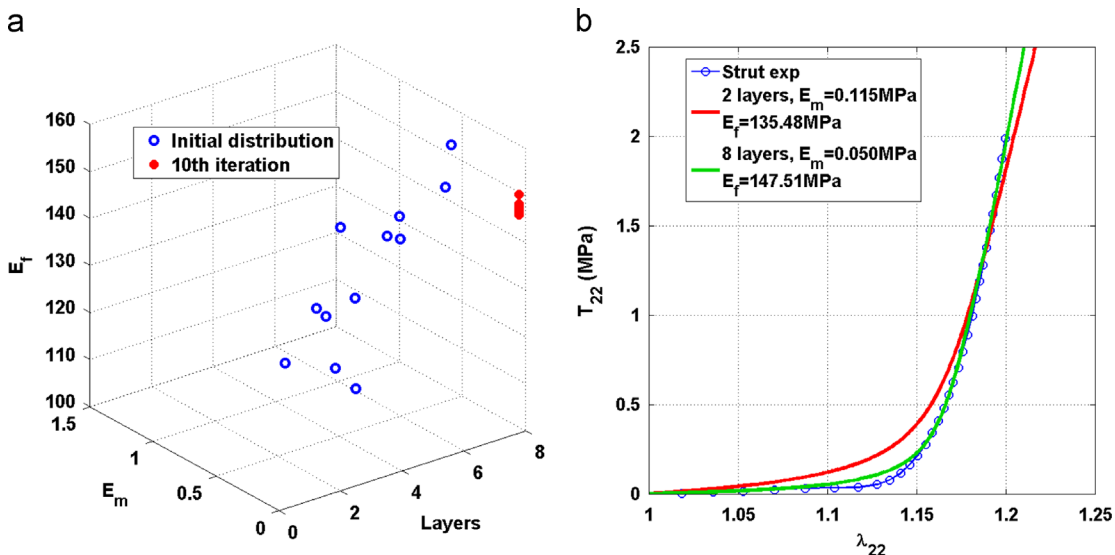


Fig. 12 – (a) Initial and final particle distributions. (b) Best initial and final simulated homogenized responses of the basal chordae tendineae.

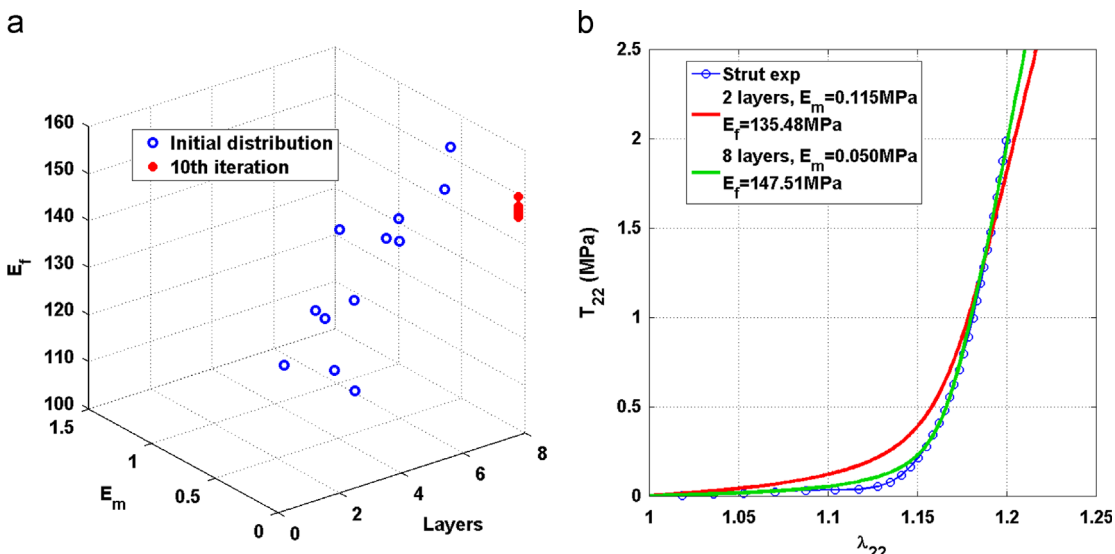


Fig. 13 – (a) Initial and final particle distributions. (b) Best initial and final simulated homogenized responses of the strut chordae tendineae.

In contrast, the optimal unit cell architecture with intact stiff layers that mimics very well the basal chordae response is more sensitive to the presence of defects, as observed in Fig. 15. In particular, while 1 fracture does not have much impact on the homogenized response, 3 breaks produce deviation which is greater than that caused by 7 fractures in the optimal marginal chordae unit cell. The response in the presence of 5 fractures fails to meet the targeted response in the stiff region to within an acceptable tolerance. The deviations only occur in the stiff region of the homogenized stress-stretch curve, thereby suggesting that the stiff layers are not effective in supporting the applied load through the shear-lag stress transfer mechanism in the presence of multiple breaks. This is observed in the normal stress distributions within intact and damaged stiff

layers, with the low normal stresses in the affected layers due to the low modulus of the matrix phase, and hence low values of shear stress. Thus the damage tolerance of the unit cell representative of the basal chordae response is limited to a total of 3 breaks per 8 stiff layers.

The ineffectiveness of the stress transfer mechanism through shear lag remains essentially the same for the unit cell that mimics the response of the strut chordae tendineae. As in the case of the basal chordae model, the low value of the matrix modulus renders the stress transfer mechanism through shear-lag ineffective as observed in the stress distributions (not shown). In summary, given that a low value of matrix modulus is required to ensure small resistance to the unfolding process of the wavy microstructures representative of basal and strut

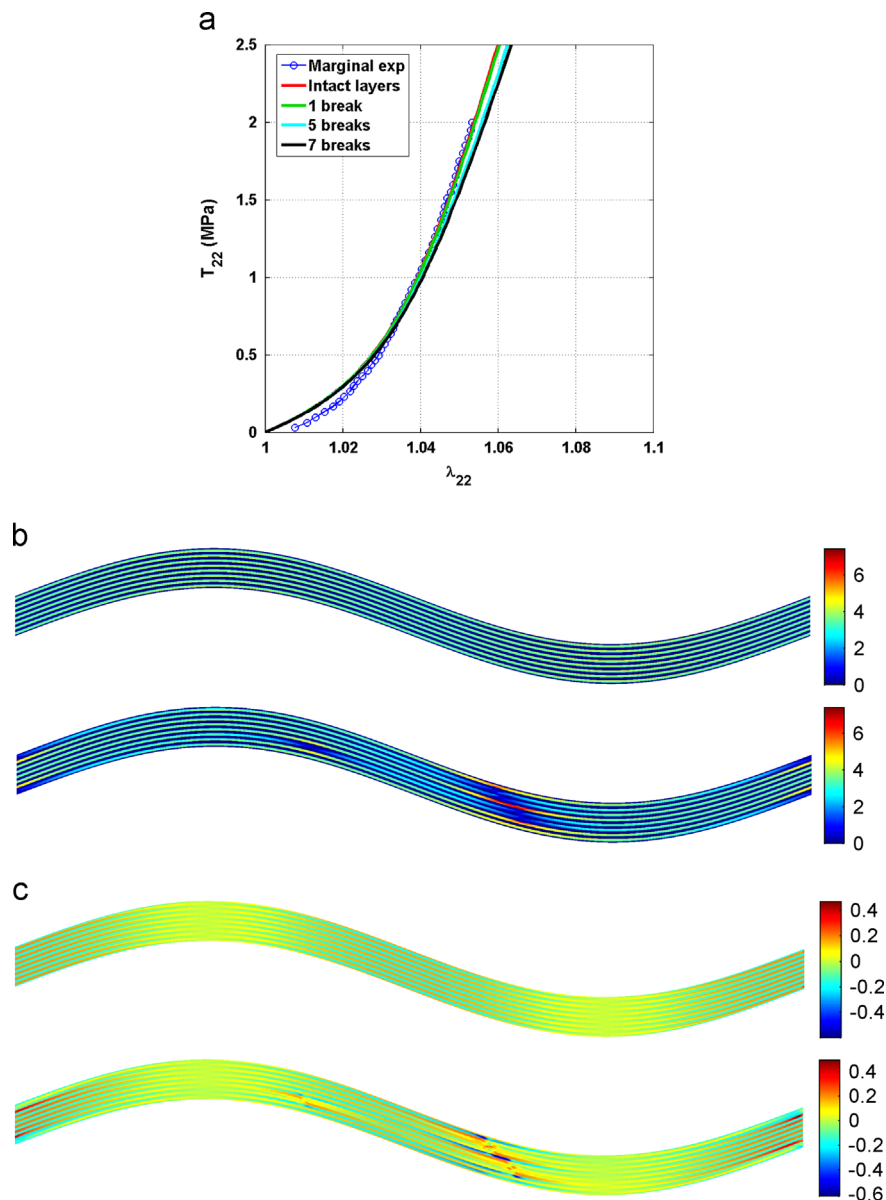


Fig. 14 – (a) Simulated homogenized response of the marginal chordae tendineae as a function of stiff layer breaks that maximize the error function. Comparison of (b) normal and (c) shear stress distributions in unit cells with intact and broken stiff layers at $\lambda_{22} = 1.05$, illustrating fracture locations.

chordae during the initial deformation stage which leads to large extensibilities, the corresponding unit cell architectures exhibit higher defect criticality relative to the marginal chordae model in the presence of multiple fractures.

5. Discussion

This study demonstrates that the stiffening response of three types of porcine mitral valve chordae characterized by complex crimped microstructures and radically different extensibilities (Liao et al., 2009) may be very accurately mimicked using the homogenization approach based on simplified two-dimensional wavy multilayer architectures with optimized geometric and layer properties. Identification of optimal properties was

achieved with the newly developed FVDAM-driven PSO algorithm that is well-suited for determining minimum objective functions in design spaces that exhibit steep gradients, cusps and multiple minima. This was the case in the two-dimensional design space defined by the amplitude and period of the chordae crimped microstructures. The PSO algorithm was verified by extensive parametric studies which also delineate the importance of geometric and material parameters of the chordae's simplified model on the initial unfolding process, the transition region and the limiting behavior defined by the fully extended bundles of collagen fibrils. These studies support the development of a new generation of synthetic chordae for mitral heart valve repair.

As is well-known, the amplitude-to-wavelength ratio plays a major role in defining the chordae extensibility (Liao and

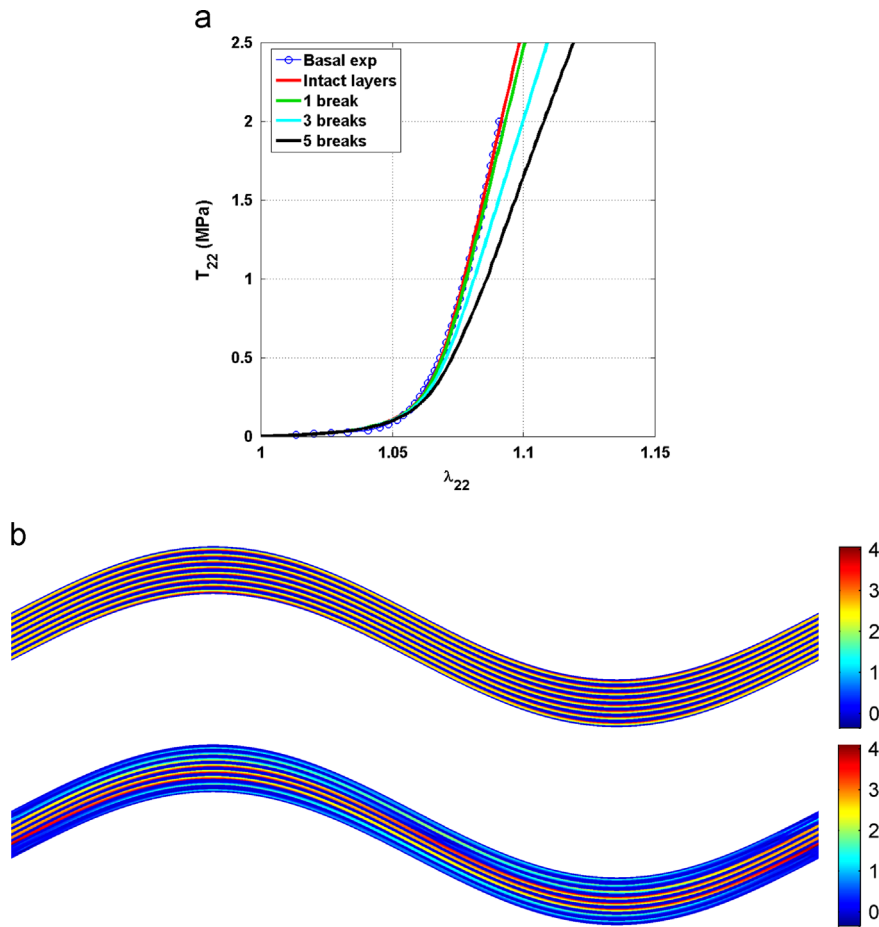


Fig. 15 – (a) Simulated homogenized response of the basal chordae tendineae as a function of stiff layer breaks that maximize the error function. **(b)** Comparison of normal stress distributions in unit cells with intact and broken stiff layers at $\lambda_{22} = 1.08$.

Vesely, 2003a). The optimal ratios of the simplified unit cell models that made possible accurate capture of the experimental response of marginal, basal and strut chordae were 0.0612, 0.0832 and 0.1352, respectively. These lie in the ranges of the actual experimentally determined values. The stiff layer thickness and the soft layer Young's modulus also play important roles during the initial unfolding process of the crimped microstructure and in the transition region, while the stiff layer modulus defines the limiting response. These must be adjusted appropriately in order to accurately capture the different shapes of the stiffening responses exhibited by the investigated chordae. Specifically, the stiff layer thickness should be on the order of the diameter of a collagen fibril for the three chordae types. This motivates the development of nano-scale films with crimped architectures in parallel with research on tissue-engineered mitral valve chordae using the principle of directed collagen gel shrinkage (Shi and Vesely, 2004). A relatively large soft layer modulus is also required to capture the initial and transition response of the marginal chordae with the smallest amplitude-to-wavelength ratio, and thus smallest extensibility. This supports the hypothesis of higher interfibrillar cross-link density for smaller diameter marginal fibrils (Liao and Vesely, 2003a), which provides greater fibril-to-fibril interaction during the uncrimping process modeled through a higher soft layer modulus. This mechanism (Fratzl et al., 1997), however, does not extend to the linear region of the limiting response in the

present model. In our case, the stiffer limiting response of the marginal chordae is accounted for through the higher extracted modulus of the stiff layers. In contrast, much smaller modulus is required to simulate the responses of basal and strut chordae with substantially greater extensibilities and much longer initial responses characterized by very low compliances. For these chordae, the soft layer modulus together with the stiff layer thickness, which defines the bending stiffness in the crest and trough regions of the wavy multilayer architecture, must be minimized in order to ensure accurate simulation of the low compliance during the unfolding of the crimped microstructure.

The soft layer modulus also plays an important role in layer-to-layer stress transfer in the presence of local fractures. The effectiveness of a fractured layer in supporting the load away from the local break through the well-known shear-lag mechanism depends on the magnitude of the matrix shear modulus which must be sufficiently high. Hence the defect criticality of optimal unit cell architectures that mimicked the marginal chordae response was relatively low in comparison with the optimal basal and strut unit cell architectures. The latter required low values of the matrix modulus to accurately capture the initial response during the unfolding process of the wavy microstructure, thereby leading to lower tolerance of local defects or higher defect criticality. These results suggest that anisotropic matrices characterized by low Young's moduli and shear moduli higher than those characteristic of isotropic

materials may be required to improve defect criticality of the latter two types of chordae.

Finally, the present model does not account for the documented time-dependent effects exhibited by the porcine mitral valve chordae (Liao and Vesely, 2004). Hence the validity of the present results is limited to the strain rate employed to generate the experimental data (Liao and Vesely, 2003a) from which the model parameters were extracted for use in the simplified unit cells. Given that most materials exhibit time-dependent behavior to a greater or lesser extent, the assessment of its impact on long-term cyclic response of synthetic chordae remains to be done. The approach employed in the previous work based on an earlier micromechanics approach (Pindera, 2004) may be employed for this purpose upon further generalization of FVDAM.

6. Summary and conclusions

An extensive homogenization-based parametric sensitivity study has demonstrated the feasibility of employing simplified, two-dimensional wavy multilayer unit cell architectures to accurately simulate the stiffening response of complex biological tissues with crimped collagen fiber microstructures such as mitral valve marginal, basal and strut chordae tendineae characterized by different amplitude-to-wavelength crimp patterns. This study has identified the roles that different geometric and material parameters play in controlling the initial, transition and limiting tensile response of these chordae tendineae types. The parametric sensitivity results support an independently conducted PSO-based optimization investigation to identify optimal geometric and material parameters that produce best fit with experimental data, demonstrating the usefulness of a non-gradient based algorithm in minimizing objective functions with steep gradients, cusps and multiple local minima.

The results also demonstrate that in certain circumstances the targeted response may be attained using more than one wavy material architecture. Moreover, defect criticality analysis of the optimal unit cell microstructures has revealed the importance of the matrix modulus in attaining the targeted response in the presence of localized stiff layer fractures. Optimal unit cell architectures characterized by relatively large matrix modulus that mimic the marginal chordae response possess substantially greater damage tolerance than unit cells representative of the basal and strut chordae. The low matrix modulus required for the low resistance during the unfolding of the wavy microstructures characterized by large extensibilities exhibited by basal and strut chordae renders the shear-lag mechanism ineffective in stress transfer from the fractured region into the intact portions of the affected and adjacent layers. This leads to loss of load-bearing capability of the fractured layers, resulting in degraded homogenized response that does not meet its target in the presence of a sufficiently large number of breaks.

Acknowledgments

The authors gratefully acknowledge the support of the Nano and Bio Mechanics Program Grant Award # CMMI-1030673.

REFERENCES

- Bensoussan, A., Lions, J.-L., Papanicolaou, G., 1978. *Asymptotic Analysis for Periodic Structures*. North Holland, Amsterdam.
- Berezovski, A., Engelbrecht, J., Maugin, G.A., 2008. *Numerical Simulation of Waves and Fronts in Inhomogeneous Solids*. World Scientific Publishing Co, New Jersey.
- Bortolotti, U., Aldo, D., Milano, A.D., Frater, R.W.M., 2012. Mitral valve repair with artificial chordae: a review of its history, technical details, long-term results, and pathology. *Annals of Thoracic Surgery* 93, 684–691.
- Browning, A., Ortiz, C., Boyce, M.C., 2013. Mechanics of composite elasmoid fish scale assemblies and their bioinspired analogues. *Journal of the Mechanical Behavior of Biomedical Materials* 19, 75–86.
- Buehler, M.J., 2006. Atomistic and continuum modeling of mechanical properties of collagen: elasticity fracture, and self-assembly. *Journal of Materials Research* 21 (8), 1947–1961.
- Cavalcante, M.A.A., Pindera, M.-J., Khatam, H., 2012. Finite-volume micromechanics of periodic materials: past, present and future. *Composites B* 43 (6), 2521–2543.
- Cavalcante, M.A.A. and Pindera, M.-J., 2013a. Generalized FVDAM theory for periodic materials undergoing finite deformations. Part I: framework. *Journal of Applied Mechanics*. <http://dx.doi.org/10.1115/1.4024406> (in press).
- Cavalcante, M.A.A. and Pindera, M.-J., 2013b. Generalized FVDAM theory for periodic materials undergoing finite deformations. Part II: numerical results. *Journal of Applied Mechanics*. <http://dx.doi.org/10.1115/1.4024407> (in press).
- Charalambakis, N., 2010. Homogenization techniques and micromechanics: a survey and perspectives. *Applied Mechanics Reviews* 63, 1–10.
- Chen, J., Peng, W., Ge, R., Wei, J., 2009. Optimal design of composite laminates for minimizing delamination stresses by particle swarm optimization combined with FEM. *Structural Engineering Mechanics* 31 (4), 407–421.
- Comninou, M., Yannas, I.V., 1976. Dependence of stress-strain nonlinearity of connective tissues on the geometry of collagen fibers. *Journal of Applied Mechanics* 9, 427–433.
- Diamant, J., Keller, A., Baer, E., Litt, M., Arridge, R.G.C., 1972. Collagen; ultrastructure and its relation to mechanical properties as a function of ageing. *Proceedings of the Royal Society of London B* 180, 293–315.
- Demirdzic, I., Martinovic, D., 1993. Finite volume method for thermo-elastic-plastic stress analysis. *Computer Methods in Applied Mechanics and Engineering* 109, 331–349.
- Federico, S., Herzog, W., 2008. Towards an analytical model of soft biological tissues. *Journal of Biomechanics* 41, 3309–3313.
- Fratzl, P., Misof, K., Zizak, I., Rapp, G., 1997. Fibrillar structure and mechanical properties of collagen. *Journal of Structural Biology* 122, 119–122.
- Freed, A.D., Doebring, T.C., 2005. Elastic model for crimped collagen fibrils. *Journal of Biomechanical Engineering* 127, 587–593.
- Gao, Y., Waas, A.M., Faulkner, J.A., Kostrominova, T.K., Wineman, A.S., 2008. Micromechanical modeling of the epimysium of the skeletal muscles. *Journal of Biomechanics* 41, 1–10.
- Garikipati, K., Goktepe, S., Miehe, C., 2008. Elastic-based strain energy functions for soft biological tissue. *Journal of the Mechanics and Physics of Solids* 56, 1693–1713.
- Grytz, R., Meschke, G., 2009. Constitutive modeling of crimped collagen fibrils in soft tissues. *Journal of the Mechanical Behavior of Biomedical Materials* 2, 522–533.
- Hill, R., 1963. Elastic properties of reinforced solids: some theoretical principles. *Journal of the Mechanics and Physics of Solids* 11, 357–372.

- Ibrahim, M., Rao, C., Athanasiou, T., 2012. Artificial chordae for degenerative mitral valve disease: critical analysis of current techniques. *Interactive Cardiovascular and Thoracic Surgery* 15, 1019–1032.
- Kastelic, J., Galeski, A., Baer, E., 1978. The multicomposite structure of tendon. *Connective Tissue Research* 6, 11–23.
- Kastelic, J., Palley, I., Baer, E., 1980. A structural mechanical model for tendon crimping. *Journal of Biomechanics* 13, 887–889.
- Kennedy, J., Eberhart, R., 1995. Particle swarm optimization. In: *Proceedings of IEEE International Conference on Neural Networks*, pp. 1942–1948.
- Khatam, H., Pindera, M.-J., 2012. Microstructural scale effects in the nonlinear elastic response of bio-inspired wavy multilayers undergoing finite deformation. *Composites B* 43 (3), 869–884.
- Liao, J., Vesely, I., 2003a. A structural basis for the size-related mechanical properties of mitral valve chordae tendineae. *Journal of Biomechanics* 36, 1125–1133.
- Liao, J., Vesely, I., 2003. Mechanical and Structural Properties of Mitral Valve Chordae Tendineae. Heart Valve Laboratory, BME, Cleveland Clinic Foundation. PPT Presentation Communicated to Engineered Materials Concepts, LLC in fulfillment of the Subcontract Requirements through the DHRP Grant No. DAMD17-01-1-0673.
- Liao, J., Vesely, I., 2004. Relationship between collagen fibrils, glycosaminoglycans, and stress relaxation in mitral valve chordae tendineae. *Annals of Biomedical Engineering* 32 (7), 977–983.
- Liao, J., Priddy, L.B., Wang, B., Chen, J., Vesely, I., 2009. Ultrastructure of porcine mitral valve chordae tendineae. *Journal of Heart Valve Disease* 18 (3), 292–299.
- Maceri, F., Marino, M., Vairo, G., 2010. A unified multiscale mechanical model for soft collagenous tissues with regular fiber arrangement. *Journal of Biomechanics* 43, 355–363.
- Peng, W., Chen, J., Wei, J., Tu, W., 2011. Optimal strength design for fiber-metal laminates and fiber-reinforced plastic laminates. *Journal of Composite Materials* 45 (2), 237–254.
- Pindera, M.-J., 2004. Micromechanics-based modeling of biological tissues using the high-fidelity generalized method of cells. In: Viney, C., Katti, K., Ulm, F.-J., Hellmich, C. (Eds.), *MRS 2004 Symposium Proceedings, Mechanical Properties of Bio-Inspired and Biological Materials*, vol. 844. Boston, MA, USA, pp. 223–234.
- Pindera, M.-J., Khatam, H., Drago, A.S., Bansal, Y., 2009. Micromechanics of spatially uniform heterogeneous media: a critical review and emerging approaches. *Composites B* 40 (5), 349–378.
- Shi, Y., Vesely, I., 2004. Characterization of statically loaded tissue-engineered mitral valve chordae tendineae. *Journal of Biomedical Material Research A* 69 (1), 26–39.
- Suquet, P.M., 1987. Elements of Homogenization for Inelastic Solid Mechanics, *Lecture Notes in Physics*, vol. 272. Springer-Verlag, Berlin, New York.
- Tang, H., Buehler, M.J., Moran, B., 2009. A constitutive model of soft tissue: from nanoscale collagen to tissue continuum. *Annals of Biomedical Engineering* 37 (6), 1117–1130.
- Versteeg, H.K., Malalasekera, W., 2007. *An Introduction to Computational Fluid Dynamics: The Finite Volume Method*. Pearson Education, Ltd., Prentice Hall, New York.